

Current Distribution in Nonequilibrium $\mathbf{J} \times \mathbf{B}$ Devices

G. S. ARGYROPOULOS, S. T. DEMETRIADES, AND A. P. KENDIG

STD Research Corporation, Pasadena, California

(Received 19 May 1967; in final form 21 August 1967)

The interdependent problems of determining the current density field and the electron temperature and number density profiles in nonequilibrium $\mathbf{J} \times \mathbf{B}$ devices are formulated realistically, and solved numerically. The two-dimensional formulation includes the important effects of thermal and concentration diffusion, thermal and velocity boundary layers, and finite reaction rates on the electrical behavior of crossed-field devices, and allows each effect to be studied separately. As a result, this study predicts and interprets the asymmetry of the current distribution that has often been reported in experimental studies. Computations in potassium-seeded nitrogen plasmas have shown that streamwise nonuniformities can be very pronounced both in the core and in the electrode boundary regions of high-current density devices. In the limiting case of instantaneous reaction rates (ionization equilibrium at the electron temperature) and instantaneous energy relaxation, current lines in the core display a striking increase in slope throughout the narrow region between the insulator segments, where they become almost perpendicular to the flow direction and much denser than in the remaining part of the core. Under these conditions, there is no evidence of current "shorting" through the boundary layer, although the T_e distribution is such that high-luminosity regions appear over the electrodes, particularly over the cathode. The general and flexible methods developed in this study allow realistic evaluation of suggested designs under various operating conditions.

Important physical mechanisms that influence the electrical behavior and design parameters of crossed-field devices (accelerators and generators) include thermal diffusion, the gasdynamic boundary layers on the walls, and relaxation effects due to finite reaction and energy transfer rates.

The problem of determining the current density field $\mathbf{J}(x, y)$ in a $\mathbf{J} \times \mathbf{B}$ geometry with segmented electrodes, can be formulated in a general and realistic mathematical model that includes the effect of these physical mechanisms. Using the conventional notation (x is the direction of the plasma velocity \mathbf{U} , y is the direction of the applied electric field \mathbf{E} , z is the direction of the applied magnetic induction \mathbf{B}), we find (see Appendix) that the current streamfunction $\Psi(x, y)$ satisfies the nonlinear¹ differential equation

$$\nabla^2 \Psi + M \partial \Psi / \partial x + N \partial \Psi / \partial y = P, \quad (1)$$

where

$$M = (\sigma/\epsilon) [(\partial/\partial x)(\epsilon/\sigma) - (\partial/\partial y)(\beta/\sigma)] \quad (1a)$$

$$N = (\sigma/\epsilon) [(\partial/\partial y)(\epsilon/\sigma) + (\partial/\partial x)(\beta/\sigma)] \quad (1b)$$

$$P = (\sigma/\epsilon) (B \nabla \cdot \mathbf{U} - \partial K_y / \partial x + \partial K_x / \partial y), \quad (1c)$$

while \mathbf{K} is an "effective" electric field due to electron temperature and pressure gradients, and defined by²

$$\mathbf{K} = -[\theta^{(1)} \nabla T_e + \theta^{(2)} \nabla T_e \times \mathbf{B} + \theta^{(3)} (\nabla T_e \times \mathbf{B}) \times \mathbf{B}] - [\beta_e^{(1)} \nabla p_e + \beta_e^{(2)} \nabla p_e \times \mathbf{B}]. \quad (2)$$

The coefficients $\theta^{(i)}$ and $\beta_e^{(i)}$ have been defined in Ref. 2. The scalar conductivity σ and the parameters β and ϵ are associated with the coefficients of Ohm's law, which

¹ Equation (1) is nonlinear because M , N , and P are strong functions of the electron temperature which in nonequilibrium devices is coupled to the current density \mathbf{J} through the electron energy equation.

² S. T. Demetriades and G. S. Argyropoulos, *Phys. Fluids* **9**, 2136 (1966).

has the form

$$\mathbf{E} + \mathbf{U} \times \mathbf{B} + \mathbf{K} = (1/\sigma) \mathbf{J} + \chi \mathbf{J} \times \mathbf{B} - \psi (\mathbf{J} \times \mathbf{B}) \times \mathbf{B}. \quad (3)$$

Specifically, in the notation of Ref. 2, $\beta \equiv \sigma \chi B$ and $\epsilon \equiv 1 + \sigma \psi B^2$. The form of Ohm's law used in this work is the one developed in Ref. 2; it corresponds to the second Chapman-Enskog approximation, includes ion currents and the effect of temperature and pressure gradients, and is valid for multicomponent, nonisothermal plasmas. (In the *first* approximation, β reduces to the commonly used Hall parameter $\omega \tau$, while ψ reduces² to the "ion-slip" coefficient. In the second approximation there is an *electronic* contribution to ψ , which is usually more important than the ion-slip term.) Our formulation shows that the parameter β/ϵ appears *in place of* $\omega \tau$ of the first-order theories. In the second approximation, β/ϵ can be 10%-20% lower than $\omega \tau$.

We see that Ohm's law and the streamfunction equation depend upon gasdynamic variables both explicitly (plasma velocity \mathbf{U} , temperature and pressure gradients) and implicitly (temperature and pressure dependence of the coefficients). Because of this dependence, the current distribution is coupled to the gasdynamic problem (i.e., the problem of determining the pressure, temperature, and velocity distributions in the device). The gas velocity and the gas temperature profiles in the electrode boundary regions can have a significant influence upon the current distribution. We have therefore included them in the formulation. This does not mean, however, that we have solved the combined electrical-and-gasdynamic problem. Instead, we obtain the best available estimates and measurements of the gas velocity and temperature profiles for a given case, and use them as inputs for the solution of the "electrical" problem. This approach is justified by the fact that neither the gas temperature nor the gas velocity can vary appreciably *in the flow*

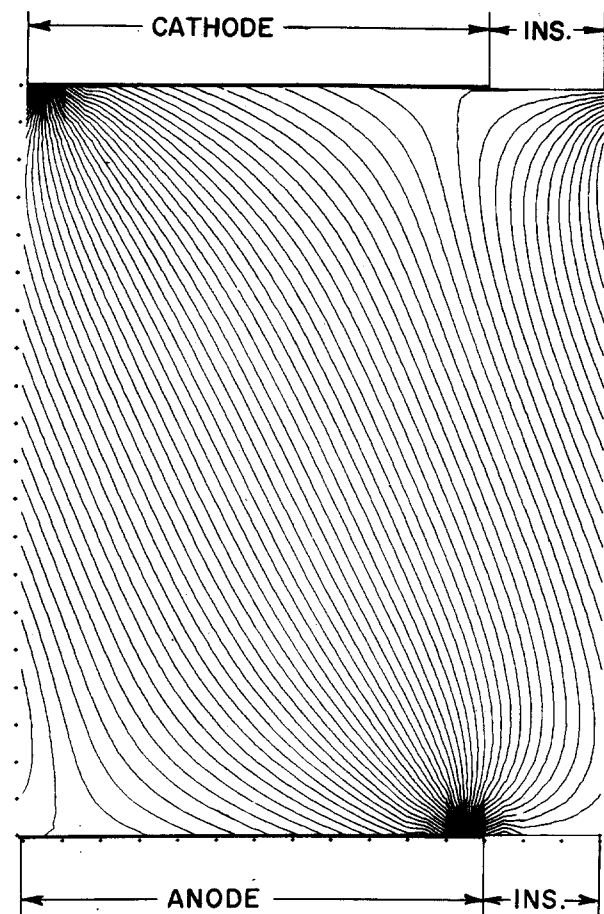


FIG. 1. Current streamlines by "constant property" calculation. Hall parameter $\beta/\epsilon = 2.6$.

direction within one electrode-pair region, and achieves our objective of evaluating the influence of these profiles on the electrical behavior, but is subject, of course, to the accuracy by which these profiles are estimated or measured.

Finally, the coefficients of Ohm's law are strong functions of the electron temperature and the plasma composition, the variations of which in nonequilibrium devices are inherently connected to the current distribution through the electron energy equation. Consequently, it is not possible in nonequilibrium $\mathbf{J} \times \mathbf{B}$ devices to uncouple the current distribution from the *electron temperature* and *number density* fields; it is necessary to solve for all these distributions simultaneously.

The electron energy equation has been used in the present study in its steady-state form, as a local balance between electron heating due to Ohmic dissipation and energy transfer due to collisions. It takes account of the heating or cooling of electrons due to thermal diffusion and, for the term that describes the energy transfer due to collisions between electrons and heavy particles, it uses the result derived by the 13-moment approximation.² For diatomic plasmas, in the range of

temperatures and power densities that we have considered, radiation losses can be neglected in the electron energy equation. We have used values for the energy loss factor of electrons in hot nitrogen that have been measured experimentally in our laboratory.³

The mathematical problem that consists of the streamfunction, electron energy and finite rate (continuity) equations, the geometry of interest, and the appropriate boundary conditions (see Appendix) has been solved numerically. The solution was based on an iteration scheme that obtains a converging sequence for the electron temperature profile. The computation starts with an arbitrary approximation for the electron temperature variation in the region of interest $T_e = T_e(x, y)$. Then, taking into consideration the *given* gasdynamic profiles for the total static pressure p and the gas temperature T_0 , we calculate the spatial variations of all plasma properties, and thus determine $M(x, y)$, $N(x, y)$ and $P(x, y)$ in Eq. (1). We distinguish two cases.

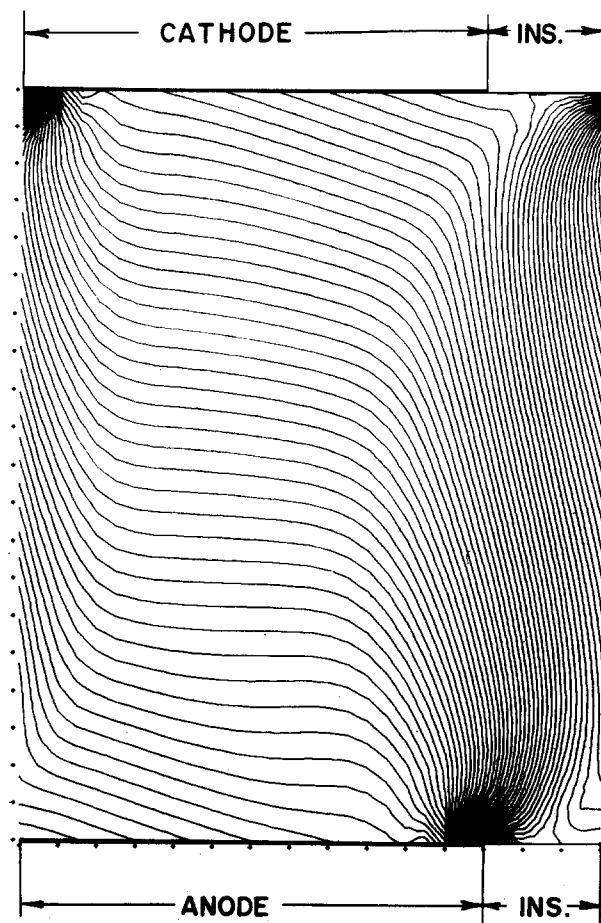


FIG. 2. Current streamlines: uniform gas temperature computation with thermal diffusion. Range of Hall parameter variation in the field: $\beta/\epsilon = 1.7-3.8$.

³ S. T. Demetriades, Phys. Review 158, 215 (1967).

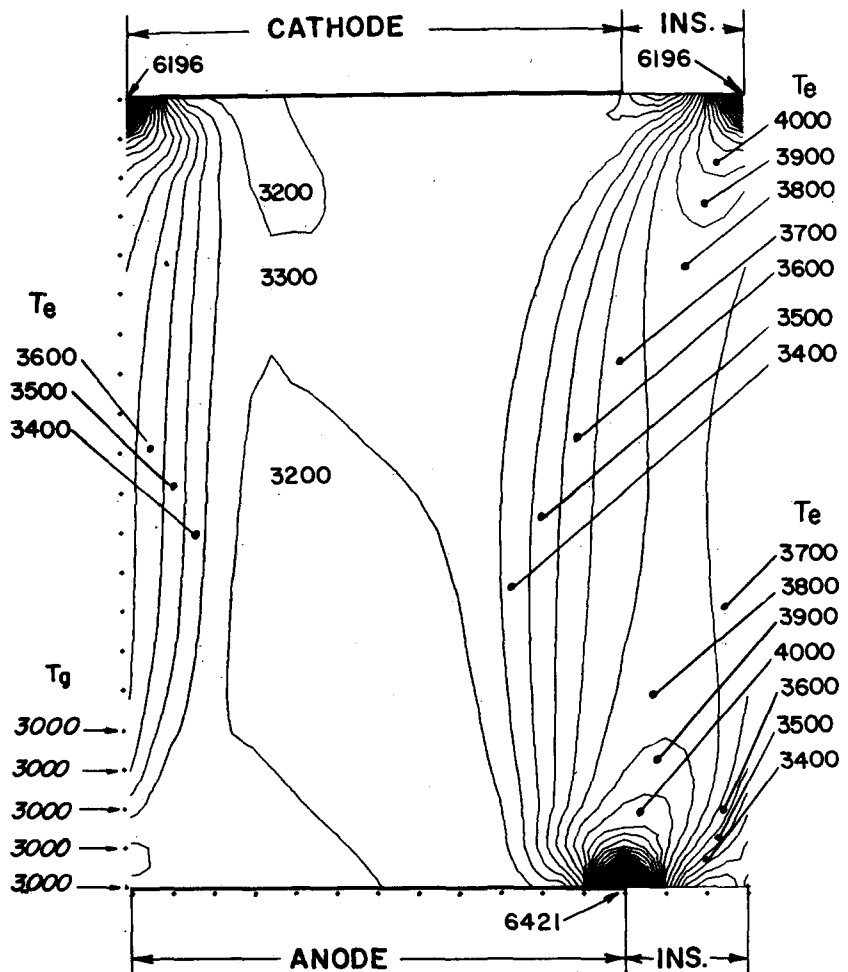


FIG. 3. Electron temperature profile (in °K); uniform gas temperature computation with thermal diffusion (corresponds to the current distribution of Fig. 2).

1. INSTANTANEOUS REACTION RATES

In this case which is valid when $Ln_e^2 \cdot r(T_e)/U \gg 1$ [where L = electrode period in meter, $r(T_e)$ = electron recombination rate coefficient, and n_e = electron number density], the continuity equations reduce to algebraic Saha equilibrium relations. Assuming ionization equilibrium at the electron temperature and dissociation equilibrium at the gas (or the electron) temperature, we can determine the number of densities of all components and thus, using the theory of Ref. 2, all plasma properties as functions of T_e , T_a , and p .

2. FINITE REACTION RATES

In this case, we need information about ionization and dissociation rates of the chemical species that constitute the plasma. Using experimental or theoretical values for these rates as functions of T_e , together with the assumed T_e profile and the given velocity profile $\mathbf{U} = \mathbf{U}(x, y)$, we can again determine the number densities of all plasma components as functions of x and y and thus find $M(x, y)$, $N(x, y)$ and $P(x, y)$.

When the obtained values of M , N , and P are substituted in Eq. (1), the latter assumes a linear elliptic

form. This elliptic equation, together with the boundary conditions, is then solved numerically with a variable mesh grid and a *direct* numerical method. In practice, *iterative* methods tend to be preferred for solving the large sparse linear systems of finite-difference equations that correspond to elliptic partial differential equations, because such methods (e.g., over-relaxation) can take advantage of the sparsity (i.e., the numerous zeros) in the matrix of the unknowns. However, iterative methods encounter serious convergence difficulties in the neighborhood of singular points. In this problem, the edges of the two conductors are singular points of the streamfunction equation, and considerable convergence difficulty in their neighborhood has been encountered in previous numerical studies, all of which have used iterative methods to solve the streamfunction equation. For example, "the number of iterations required for the determination of a single J distribution varies from 500 to 2000."⁴ We have avoided these difficulties and also greatly reduced the computing effort by using a *direct* method of solution, i.e., by inverting the matrix of the unknowns. We have done this by

⁴L. L. Lengyel, Eighth Symposium on Engineering Aspects of Magnetohydrodynamics, Stanford (1967).

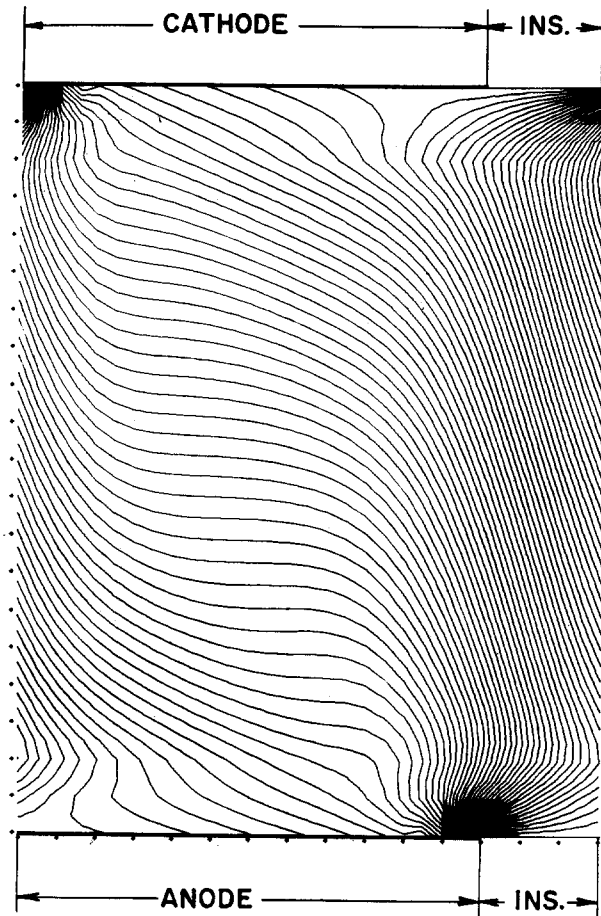


FIG. 4. Current streamlines: boundary-layer computation with thermal diffusion. Range of Hall parameter variation in the field: $\beta/\epsilon = 1.6-4.5$.

inventing a recursive elimination procedure that takes full advantage of the sparsity of the matrix for this problem and allows us to invert a matrix of order n instead of order n^2 when treating an $n \times n$ grid. Our approach is quite straightforward and demonstrates the advantages and limitations of direct methods; details will be published in a company report.

Finally, after the current density field has been determined, we use the *electron energy equation* to compute algebraically the new electron temperature profile that is consistent with it, and use this computed T_e profile as the input to the next iteration cycle.

This procedure has been found to converge over a fairly wide range of operating conditions. Typical results are illustrated in Figs. 1-7. They all refer to a nitrogen gas flow seeded with 0.5% potassium, and have been computed under the assumption of instantaneous reaction rates. The channel geometry and operating conditions are: conductor length $l_c = 12$ mm, insulator length $l_i = 3$ mm, electrode period $L \equiv l_i + l_c = 15$ mm, interelectrode distance $D = 20$ mm, magnetic induction $B = 2$ Wb/m², average current density $\langle J_y \rangle = 30$ A/cm², gas pressure $p = 0.5$ atm, gas temperature

in the core $T_0 = 3000^\circ\text{K}$. The assumed *gas temperature* variation $T_0(y)$ in the boundary layer is indicated in italics on Figs. 3, 5, and 7. (The computation has started approximately one electron mean free path away from the wall surface.)

Our work has led to the following conclusions:

(1) Thermal diffusion is a significant factor in non-equilibrium $\mathbf{J} \times \mathbf{B}$ devices, particularly accelerators, because of the severe electron temperature and pressure gradients that can be generated in these devices. The direction of these gradients near the anode is different than their direction near the cathode, and therefore, these gradients tend to *increase* the effective electric field [left-hand side of Eq. (3)] near one electrode, and to *decrease* it near the other. As a consequence, these gradients lead to *asymmetrical*⁵ current distributions in the channel, and different current concentrations on the anodes than on the cathodes. Asymmetrical behavior has been repeatedly reported in experimental observations, whereas previous theories,⁶⁻¹¹ having omitted this effect as well as the effect of finite reaction rates, had predicted centrally symmetric distributions. Note that Refs. 6-8 have neglected all non-uniformities in the streamfunction equation and have solved Laplace's equation; such analyses are known as "constant property" calculations.

(2) A second physical mechanism that contributes significantly to asymmetrical behavior in crossed-field channels is the influence of finite reaction rates. As the plasma moves downstream, it undergoes, within the length L of one electrode region, ionization, dissociation, and recombination at finite rates, and this leads to an asymmetrical distribution of the plasma properties. The hot region at the edge of the one electrode tends to smear downstream, and the hot region near the edge of the other electrode tends to become more concentrated.

(3) Extensive calculations of the current density field in potassium-seeded nitrogen plasmas have shown that when reaction rates are fast and the gas velocity U relatively low, there is *no* big axial current in those regions; in other words there is no evidence of current "shorting" through the boundary layer. It should be emphasized that the high-glow regions that are observed visually need not be taken to coincide with the

⁵ The symmetry referred to here is a central symmetry, or point symmetry, with respect to the point P of the centerline of the channel that is defined by the intersection of two "diagonal" lines, the one connecting the upstream edge of the anode to the downstream edge of the cathode and the other the downstream edge of the anode to the upstream edge of the cathode. Note that in each electrode pair region, there are two such points P , one between the conductor segments and the second between the insulator segments.

⁶ H. Hurwitz, R. W. Kilb, and G. W. Sutton, *J. Appl. Phys.* **32**, 205 (1961).

⁷ J. C. Crown, United Aircraft Corp. Rept. R-1852-2 (1961).

⁸ Z. N. Celinski and F. W. Fischer, *AIAA J.* **4**, 421 (1966).

⁹ J. L. Kerrebrock, *AIAA J.* **4**, 1938 (1966).

¹⁰ A. Sherman, *Phys. Fluids* **9**, 1782 (1966).

¹¹ D. A. Oliver and M. Mitchner, *AIAA J.* **5**, 1424 (1967).

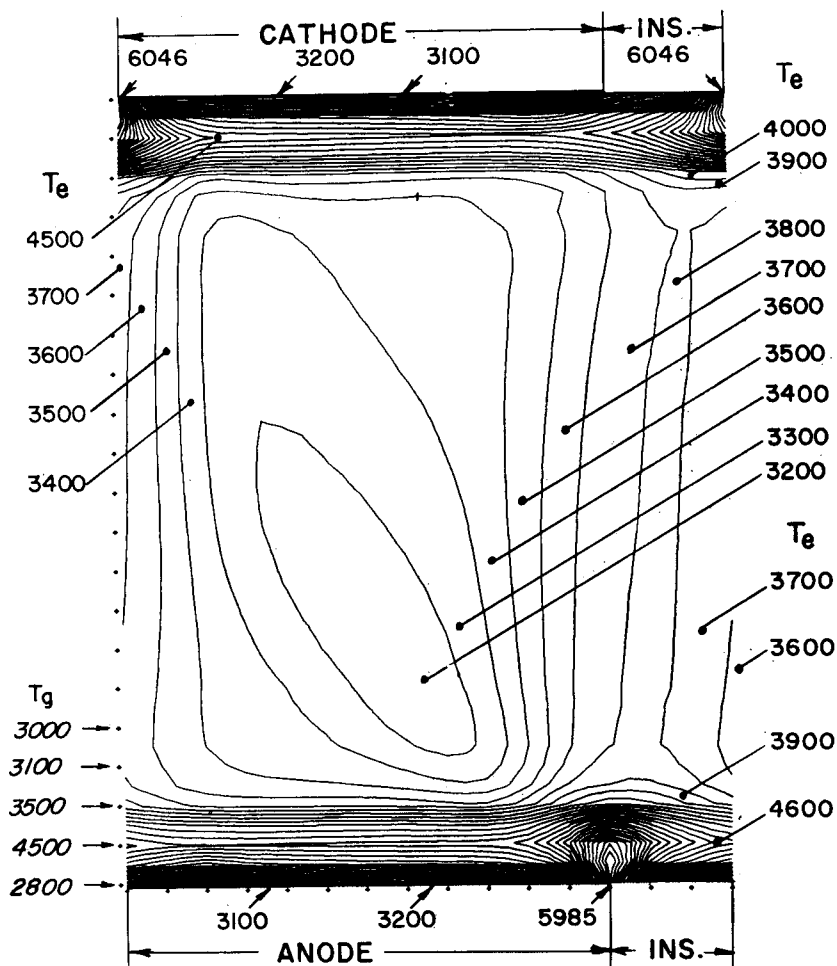


FIG. 5. Electron-temperature profile (in °K): boundary-layer computation with thermal diffusion (corresponds to the current distribution of Fig. 4).

actual path of the current over the entire region. Plots of the electron temperature contours in the computed geometries (e.g., Figs. 3, 5, and 7) over a wide range of static pressures and temperatures indeed display the visually observed behavior: the high-temperature region extends over almost the whole surface of the one electrode (the cathode or the anode depending on whether the device is an accelerator or a generator), and then quite abruptly dips vertically from the downstream end of that electrode to the downstream end of the second electrode, without extending over the remaining part of the second electrode's surface. Comparison of these plots with the corresponding current streamfunction plots (e.g., Figs. 2, 4, and 6, respectively) illustrates that the regions of highest luminosity (or temperature) do not necessarily coincide with the current path from anode to cathode of each electrode pair. In fact, the visual observation that in accelerators the current goes from the anode of one electrode pair to the cathode of the next downstream pair is shown by these computations to be a quite understandable optical illusion.

(4) For high values of the ratio β/ϵ and of the mean current density $\langle J_y \rangle$, the current distribution in Faraday devices can display pronounced streamwise nonuni-

formities both in the core and in the electrode boundary regions. In the region of the core that is bounded (in the y direction) by the two conductor segments, the current lines can be almost parallel to the flow direction. However, as we proceed towards the (usually narrow) region of the core that is bounded by the insulator segments, we observe a striking increase in the slope of the current streamlines, which now become almost perpendicular to the flow direction and much denser. In other words, the current density is high in the same region where it is perpendicular to the flow direction. This confirms the desirability of reducing the length of the conductor segment for more efficient $J \times B$ coupling and shorter channels, as has already been pointed out by Demetriades.^{12,13}

In our computations, the influence of the different physical mechanisms can be investigated separately by suppressing appropriate coefficients. Thus, Figs. 6 and 7 have been obtained by suppressing the effect of

¹² S. T. Demetriades, A. P. Kendig, G. S. Argyropoulos, A. N. Kontaratos, and N. W. Gebbie, Tech. Rept. AFFDL-TR-65-132, Air Force Flight Dynamics Laboratory, Wright-Patterson AFB, Ohio (February 1966).

¹³ S. T. Demetriades, *Third Symposium on Engineering Aspects of Magnetohydrodynamics, University of Rochester, March 1962, Proceedings* (Gordon and Breach Science Publishers, Inc., 1963), pp. 507-525.

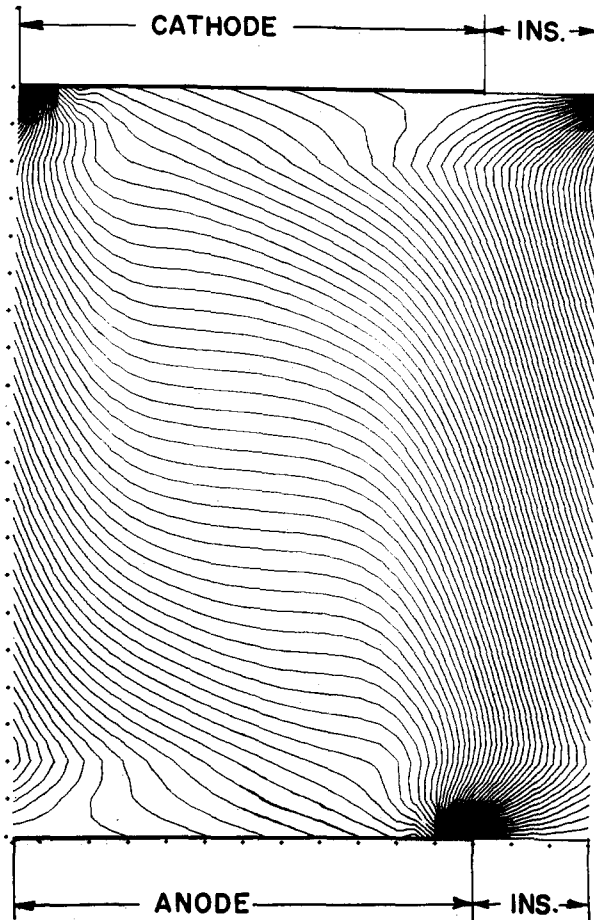


FIG. 6. Current streamlines: boundary layer computation without thermal diffusion. Range of Hall parameter variation in the field: $\beta/\epsilon = 1.6-4.1$.

electron temperature and pressure gradients, but maintaining the variation of the gas temperature in the boundary layer. Comparison with Figs. 4 and 5, respectively, shows the effect of the electron temperature and pressure gradients; without them, the distributions become again centrally symmetric (Figs. 6 and 7). We do not present figures showing the effects of finite reaction rates qualitatively described above because there exist some doubts on the actual magnitudes of the reaction rate constants in these mixtures at high electron temperatures.

The theoretical results presented in Figs. 2-6 are in remarkable agreement with previous experiments¹⁵⁻¹⁷

¹⁴ S. T. Demetriades, Second Symposium on Engineering Aspects of Magnetohydrodynamics, Philadelphia, Pa., March 1961; *Engineering Aspects of Magnetohydrodynamics*, C. Mannal and N. W. Mather, Eds. (Columbia University Press, New York 1962), pp. 19-44.

¹⁵ S. T. Demetriades and R. W. Ziemer, *Phys. Fluids* 4, 1568 (1961).

¹⁶ S. T. Demetriades and P. D. Lenn, *AIAA J.* 1, 234 (1963).

¹⁷ S. T. Demetriades and R. W. Ziemer, *Magnetohydrodynamics*, A. B. Cambel, T. P. Anderson, and M. M. Slawsky, Eds. (Northwestern University Press, Evanston, 1962), pp. 185-205.

and with the earlier phenomenological theory of Demetriades *et al.*¹⁸⁻²¹ Figure 1 gives the result of the so-called "constant property" analysis for the same conditions, and has been included for purposes of comparison. As indicated by Fig. 1, "constant property" analyses predict that perturbations due to the segmented electrodes are limited to the regions near the anode and cathode, the current distribution in the largest portion of the duct being fairly uniform. On the other hand, our work has shown (Figs. 2, 4, and 6) that the current distribution in nonequilibrium devices can be highly nonuniform even in the core, the variation of both the magnitude and the slope of the current density \mathbf{J} with respect to x being of particular significance. Although some success has been reported²² in describing *over-all* characteristics of $\mathbf{J} \times \mathbf{B}$ accelerators on the basis of "constant property" analyses, it is clear that such analyses are not always sufficient to describe the local electrical behavior of nonequilibrium $\mathbf{J} \times \mathbf{B}$ devices and that the methods of the present study may be used to obtain valid design information for such devices.

ACKNOWLEDGMENT

The research reported in this paper has been sponsored by Arnold Engineering Development Center.

APPENDIX

1. Streamfunction Equation

Equation (1) of the text has been derived by using the steady-state field equations

$$\nabla \times \mathbf{E} = 0, \quad (\text{A1})$$

$$\nabla \cdot \mathbf{J} = 0, \quad (\text{A2})$$

and operating on Ohm's law with the *curl* operator.

In the two-dimensional geometry of interest to us, Ohm's law [Eq. (3) of the text] can be written in the form

$$\mathbf{E} + \mathbf{U} \times \mathbf{B} + \mathbf{K} = (\epsilon/\sigma)\mathbf{J} + (\beta/\sigma)\mathbf{J} \times \mathbf{e}_z, \quad (\text{A3})$$

where

$$\beta \equiv \sigma \chi B, \quad (\text{A4})$$

$$\epsilon \equiv 1 + \sigma \psi B^2, \quad (\text{A5})$$

¹⁸ S. T. Demetriades, G. L. Hamilton, R. W. Ziemer, R. W. Jarl, and P. D. Lenn, *Progress in Astronautics and Aeronautics*, E. Stuhlinger, Ed. (Academic Press Inc., New York, 1963), Vol. 9, pp. 461-511.

¹⁹ S. T. Demetriades, *Physico-Chemical Diagnostics of Plasmas*, T. P. Anderson *et al.*, Eds. (Northwestern University Press, 1964), p. 297.

²⁰ A. N. Konaratos and S. T. Demetriades, *Appl. Sci. Res.* 11, Sec. B (1965).

²¹ S. T. Demetriades, *Astronautics* 7, No. 3, p. 21 and No. 4, p. 40 (March and April 1962).

²² D. R. Wilson and L. E. Rittenhouse, Fifth Hypervelocity Techniques Symposium, University of Denver (1967).

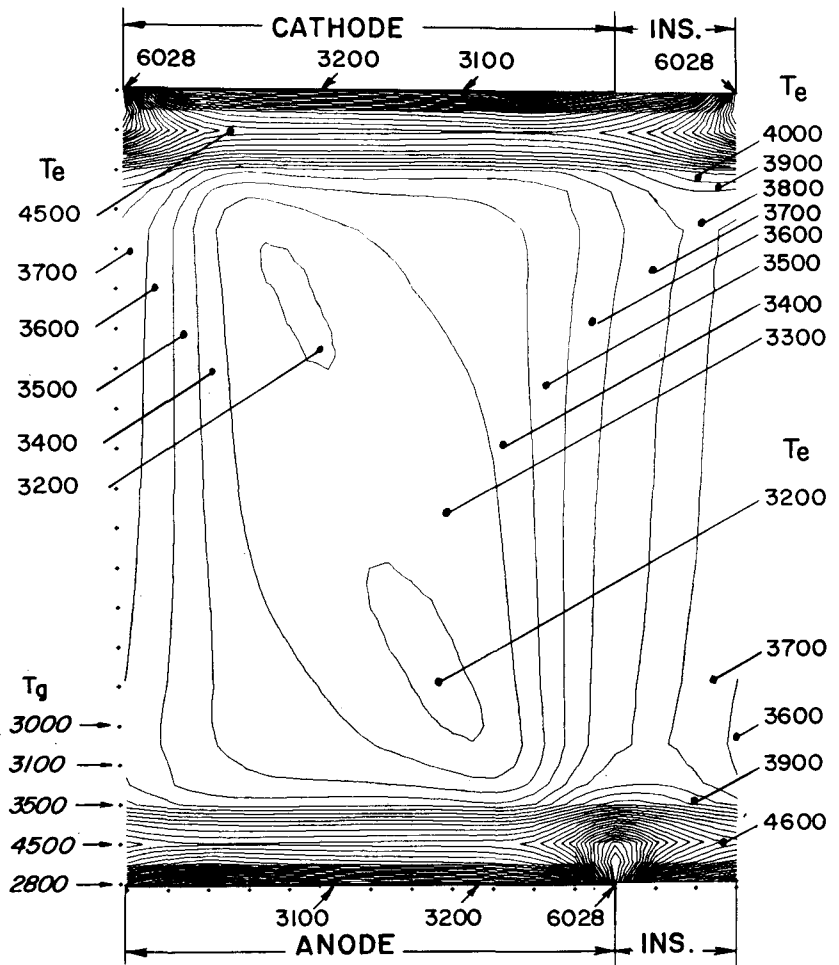


FIG. 7. Electron-temperature profile (in °K): boundary-layer computation without thermal diffusion (corresponds to the current distribution of Fig. 6).

and \mathbf{e}_z is the unit vector in the magnetic field direction. Under the operating conditions of practical $\mathbf{J} \times \mathbf{B}$ devices, the magnetic Reynolds number is much smaller than unity and the induced magnetic field can be neglected.

The current density $\mathbf{J}(x, y)$ is defined in terms of the streamfunction $\Psi(x, y)$ as

$$\mathbf{J} \equiv \nabla \times (\Psi \mathbf{e}_z), \tag{A6}$$

so that when we take the *curl* of Eq. (A3) we find

$$\begin{aligned} \nabla \times (\mathbf{U} \times \mathbf{B} + \mathbf{K}) \\ = \nabla \times [(\epsilon/\sigma) \nabla \times (\Psi \mathbf{e}_z) + (\beta/\sigma) (\nabla \times \Psi \mathbf{e}_z) \times \mathbf{e}_z]. \end{aligned} \tag{A7}$$

Projection of the vectorial Eq. (A7) on the z axis yields Eq. (1) of the text.

2. Geometry and Boundary Conditions

The geometry of interest is *one* electrode-pair region in the main part of a multielectrode channel. We are not concerned with inlet or exit effects. We have thus used periodic conditions with respect to x , namely

$$\begin{aligned} \mathbf{J}(x, y) &= \mathbf{J}(x+L, y), \\ T_e(x, y) &= T_e(x+L, y), \end{aligned} \tag{A8}$$

where L is the electrode period.

The boundary conditions on the electrode walls are:

(a) on the conductor $E_x = 0$, or, from Eq. (A3),

$$\begin{aligned} K_x &= (\epsilon/\sigma) J_x + (\beta/\sigma) J_y \\ &= (\epsilon/\sigma) [\partial \Psi / \partial y - (\beta/\epsilon) (\partial \Psi / \partial x)]. \end{aligned} \tag{A9}$$

(b) On the insulator $J_y = 0$, or

$$\Psi = \text{const.} \tag{A10}$$